Journal of Solid State Chemistry 183 (2010) 1829–1834

Contents lists available at ScienceDirect

Journal of Solid State Chemistry

journal homepage: www.elsevier.com/locate/jssc

Post-treatment and characterization of novel luminescent hybrid bimodal mesoporous silicas

Yuzhen Li, Jihong Sun*, Xia Wu, Li Lin, Lin Gao

Department of Chemistry and Chemical Engineering, College of Environmental & Energy Engineering, Beijing University of Technology, Beijing 100124, P.R. China

ARTICLE INFO

Article history:
Received 20 February 2010
Received in revised form
21 May 2010
Accepted 22 May 2010
Available online 2 June 2010

Keywords:
Post-treatment
Luminescent
Hybrid materials
Bimodal mesoporous silica

ABSTRACT

A novel luminescent hybrid bimodal mesoporous silicas (LHBMS) were synthesized via grafting 1,8-Naphthalic anhydride into the pore channels of bimodal mesoporous silicas (BMMs) for the first time. The resulting samples were characterized by powder X-ray diffraction (XRD), N_2 adsorption/desorption measurement, Fourier transform infrared spectroscopy (FT-IR), Transmission electron microscopy (TEM), UV–vis absorption spectroscopy, and Photoluminescence spectroscopy (PL). The results show that 1,8-Naphthalic anhydride organic groups have been successfully introduced into the mesopores of the BMMs and the hybrid silicas are of bimodal mesoporous structure with the ordered small mesopores of around 3 nm and the large mesopores of uniform intra-nanoparticle. The excellent photoluminescent performance of LHBMS has a blue shift compared to that of 2-[3-(triethoxysilyl) propyl-1 H-Benz [de]isoquinoline-1, 3(2 H)-dione, suggesting the existence of the quantum confinement effectiveness.

© 2010 Elsevier Inc. All rights reserved.

1. Introduction

Recently, the design of systems in controlled release and drug delivery has excited much interest, and most of the people have tried to find some materials as supports of drugs to control their release and carry delivery [1,2], however, the toxicity of the above mentioned supports has been a major problem [3,4]. Therefore, to find a good material which is non-toxic is one of the key points in the research of drug-carrying nowadays. Since the discovery of mesoporous silicas in 1992 [5], functionalized mesostructural materials have been studied extensively due to their potential applications in several fields, such as adsorption [6], sensors [7], catalysis [8], optoelectronic nanodevices [9], and so on.

Recently, mesostructural silicas have been researched as drug-delivery vehicles, owing to their unique properties, such as non-toxic nature and good biocompatibility [10]. With well-defined mesopore channel with around 3 nm and controllable particle size in the range of 20–100 nm, the bimodal mesoporous silicas (BMMs) were developed in our research group, which are recently used for controlling release and drug delivery support [11].

In the progress of carrying drug, how to track and even diagnose the effectiveness of the drug delivery is the focal point to the success of this research, namely, the drug delivery support must be functionalized by fluorescent dyes with characteristic spectra. Up to now, only few contributions have been published [12–14]. Some groups proposed the luminescent nanoparticles such as quantum dots (QDs) to target cancer cells in biomarking [15–19]. For instance, Wu group [16] has used QDs linked to immunoglobulin G and streptavidin to label the breast cancer, and the results indicate that QD-based probes are specific for the intended targets and are brighter, which is a promising luminescent material for fluorescence-based applications, however, it has relatively unstable luminescence spectra compared with traditional organic fluorophore.

It is well known that derivatives of 1,8-Naphthalic anhydride, 1, 4, 5, 8-naphthalene have been widely used in optical devices and light-emitting materials, owing to their interesting photophysical properties [20]. By combining the advantages of 1,8-Naphthalic anhydride and the BMMs, herein, we report the post-treatment of novel organic–inorganic hybrid material. Firstly, the BMMs would be modified by (3-Aminpropyl) triethoxysilane (APTES), and then 1,8-Naphthalic anhydride was grafted on the mesopore surface of BMMs.

With the help of various analytical methods, the characterization and related photoluminescence mechanism of the obtained 1,8-Naphthalic anhydride-containing mesoporous hybrid silicas are discussed in detail.

2. Experimental section

2.1. Chemicals

Cetyltrimethylammonium bromide commonly (CTAB) was obtained from Beijing Chemical Factory. Ammonia and tetraethyl

* Corresponding author. Fax: +86 010 67391983.
E-mail address: jhsun@bjut.edu.cn (J. Sun).

0022-4596/$ - see front matter © 2010 Elsevier Inc. All rights reserved.
doi:10.1016/j.jssc.2010.05.027

orthosilicate (TEOS) were provided by Beijing Yili Chemical Factory. APTES and 1,8-Naphthalic anhydride were supplied by Alfa Aesar Company. N, N-dimethyl formamide (DMF) and tetrahydrofuran (THF) were purified under reduced pressure. All the materials were all A.R. grade. Doubly distilled water was used in all experiments.

2.2. Synthesis of BMMs

In a typical preparation process, CTAB (2.6115 g) was stirred with 104 ml of doubly distilled water at room temperature until it fully dissolved. When it became a clear homogeneous solution, TEOS (8 ml) was then introduced drop wise under vigorous stirring. After a few minutes, a white gel began to form. Following the addition 4 ml of ammonia immediately, the viscosity of the mixture gradually increased, turning into a white gel. This gel was repeatedly washed with doubly distilled water for several times and filtered. Then the mixture was dried at 120 °C for 3 h. To remove the surfactant, the resultant precipitate was calcined from room temperature to 550 °C with a heating rate of 5 °C/min. Then the temperature was held constant at 550 °C for 6 h.

2.3. Synthesis of APTES-BMMs

The APTES-BMMs was prepared as follows (seen in Scheme 1): firstly, the BMMs was heated to 150 °C and kept at that temperature for 5 h to remove physisorbed water. Then 0.5 g of BMMs was dissolved in 50 ml dried THF under vigorous stirring at 25 °C. About 0.586 ml APTES was added drop wise to the mixture under continuous stirring for 10 min. After stirring for 5 h, the resulting functionalized samples were collected by filtration, and washed for three times by petroleum ether to remove the unreacted APTES and subsequently dried at 80 °C for 4 h, yielding a fine pale yellow powder.

2.4. Synthesis of luminescent hybrid bimodal mesoporous silica (LHBMS)

The LHBMS was prepared as follows (seen in Scheme 2): a solution of 0.25 g APTES-BMMs in 25 ml dried DMF was placed in a 100 ml three-necked round-bottom flask equipped with a condenser, a thermometer, and an inlet for nitrogen, respectively, and the desired amount of 1,8-Naphthalic anhydride was added to the stirred mixture. The weight ratios of the constituents in the start synthesis progress were W (1,8-Naphthalic anhydride): W (APTES-BMMs)=X: 1(X=5% (wt), 10% (wt), 20% (wt), respectively). After stirring for 5 min at 25 °C and then heating at 130 °C for 3 h in an oil bath under nitrogen atmosphere, it was found that the color of the mixture turned into orange quickly. After cooling to room temperature, The resultant precipitates were collected by filtration, washed using acetic acid to remove excess 1,8-Naphthalic anhydride and then dried overnight at 150 °C. Thus, the LHBMS composite was produced, which denoted LHBMS-5, LHBMS-10, and LHBMS-20, respectively.

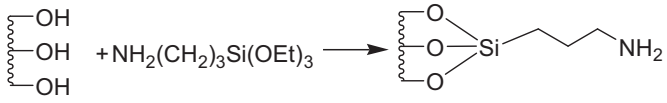

Scheme 1. A schematic representation of the modification process.

2.5. Characterization

The X-ray diffraction (XRD) patterns were recorded with a BRUKER/AXS D8 ADVANCE diffractometer at a scanning rate of 0.5°/min in 2θ ranging from 0.6°–10° with Cu$K\alpha$ radiation (λ=0.15418 nm), and the accelerating voltage was set at 35 kV with a 20 mA flux. The transmission electron microscopy (TEM) was performed on an electron microscope (JME-2010 F) under 200 kV accelerating voltage. The Fourier transform infrared (FT-IR) spectra were observed on TENSOR27 BRUKER using a KBr disk. The UV–vis spectra were carried out in the wavelength range of 200–800 nm with a double-beam UV-2450 spectrophotometer by using ethanol aqueous solution as reference. The photoluminescence spectroscopy (PL) was obtained on F7000 luminescence spectrometer equipped with a Xenon lamp of 450 W as an excitation light source. The nitrogen adsorption/desorption isotherms at −196 °C were obtained using a Micromeritics ASAP 2000 system. All the samples were outgassed at 90 °C overnight prior to gas adsorption. The corresponding pore size distribution of all samples was calculated by the BJH (Barrett–Joyner–Halenda) model on the basis of desorption branches.

3. Results and discussion

3.1. XRD analysis

The XRD patterns of samples: a (BMMs), b (APTES-BMMs), and c (LHBMS-10) are shown in Fig. 1. As can be seen, the samples all display the characteristic (1 0 0) diffraction peak of the mesoporous structure at 2θ in the range of 1.8°–2°, indicating

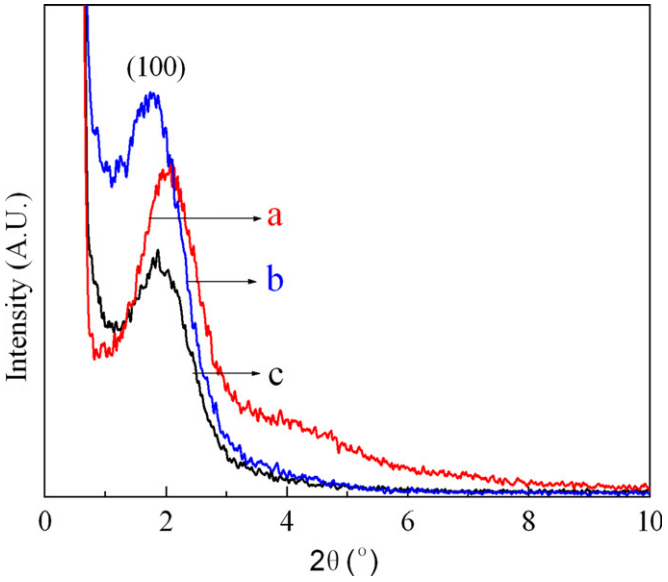

Fig. 1. XRD patterns of samples, (a) BMMs, (b) APTES-BMMs, and (c) LHBMS-10.

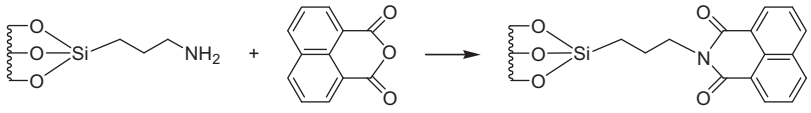

Scheme 2. A schematic representation of the grafting process.

that the ordered pore channel arrangement of all the samples has not been destroyed. However, as compared with Fig. 1a for BMMs, the (1 0 0) position of Fig. 1b for APTES-BMMs, and Fig. 1c for LHBMS-10 has shifted to a lower angle with a value of *d*-spacing from 4.345 nm to 4.934 nm to 4.617 nm, respectively, due to the location of the guest species to the pore surface of BMMs [10,11]. On the other hand, in comparison with BMMs (seen in Fig. 1a), the (1 0 0) peak intensity of LHBMS-10 (Fig. 1c) decreases obviously, implying the disordered mesostructure, which could be ascribed to the random distribution of functional groups during the process of modification and grafting (seen in Scheme 1 and Scheme 2) [21], which is in good agreement with other hybrid materials reported in the literatures [22,23]. In addition, the (1 0 0) peak intensity of the APTES-BMMs in the presence of amine groups (Fig. 1b) is higher than that of BMMs (Fig. 1a), the main reason is that the mesoporous may be restructured in the modification stage.

As seen in Fig. 2, it can be found that the intensity of the 100 diffraction peaks decreases along with increasing 1,8-Naphthalic anhydride amount, suggesting that the mesoporous structural ordering degree of the LHBMS decreases. Meantime, the *d*-spacing value of the (1 0 0) diffraction peak increases in turn from 4.345 nm for sample a (in Fig. 2a) to 4.713 nm for sample b (in Fig. 2b), 4.721 nm for sample c (in Fig. 2c), and 4.787 nm for sample d (in Fig. 2d), respectively, suggesting that the pore wall of the hybrids becomes gradually thicker with increasing amount of 1,8-Naphthalic anhydride than that of the BMMs. Further results could be given in the following section.

3.2. TEM analysis

The TEM images of the BMMs (a), APTES-BMMs (b), and LHBMS-10 (c) are displayed in Fig. 3, which clearly show a large number of uniform mesopores with pore size of about 3 nm, providing further evidence that the mesoporous structural integrity was maintained, even that after the incorporation of 1,8-Naphthalic anhydride (in Fig. 3c for sample c), which is in good agreement with the conclusion from the XRD patterns. At the meantime, the morphology of all samples presents spherical particle, in which geometric size increases from 20 nm for sample a, to 25 nm for sample b, and 35 nm for sample c, respectively.

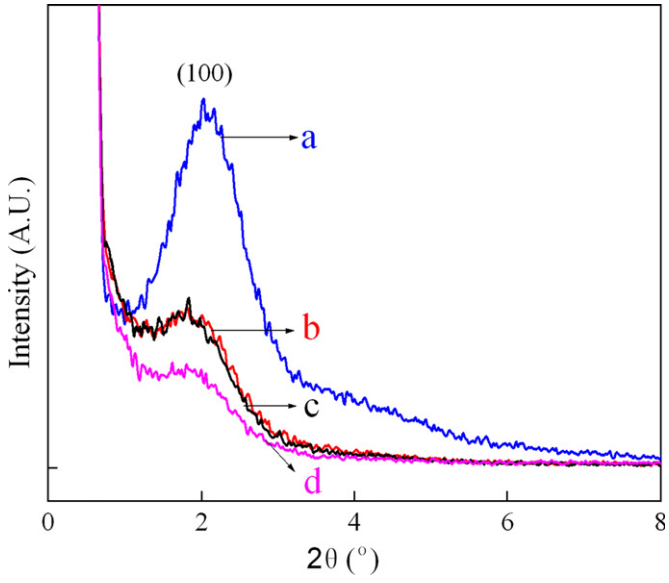

Fig. 2. XRD patterns of BMMs powder doped with different 1,8-Naphthalic anhydride amounts (a) 0%, (b) 5%, (c) 10%, and (d) 20%.

3.3. N_2 sorption analysis

The N_2 adsorption/desorption isotherms of the BMMs (a), APTES-BMMs (b), and LHBMS-10 (c) are shown in Fig. 4, and their texture parameters are given (insert). As displayed in Fig. 4, the samples all show reversible type IV adsorption/desorption isotherms, which exhibit two inflections, indicating that all the samples are in the presence of bimodal mesopore. As we can see from the Fig. 4a, the first step of isotherm ascribed to the nitrogen capillary condensation at a relative pressure range of 0.35–0.4 P/P_0, corresponding to the small mesopore with mean pore size of ca. 2.9 nm, indicative of framework-confined mesopores [21], the second one is found at 0.7–0.9 P/P_0 of type IV with an obvious H_1-type hysteresis loop, which is steeper than the first one, clearly meaning that the large mesopores with narrow pore size distribution centered at ca. 20 nm.

Compared to the three isotherms of samples (a–c) in Fig. 4, it is clearly shown that the adsorbed amount of samples a, b, and c gradually decreases in the P/P_0 value of the inflection point on the desorption branch of the isotherms, indicating that their BET surface areas have been decreased, due to the grafting of the surface of BMMs with the functional groups. On the other hand, the position of the inflection point of the isotherm is related to a diameter in the mesopore range [24]. The adsorption branches of isotherms for all samples reveal an inflection at a relative pressure value of about 0.42, suggesting that these samples have similar small pore size of around ca. 2.9 nm (seen in Fig. 4 insert), which is in good agreement with the conclusion from the XRD patterns and TEM images.

Meanwhile, the points of second inflection on the adsorption branches of isotherm for samples a, b and c show the increase at a relative pressure value of about 0.80, 0.78, and 0.75, respectively, implying that the large mesopore size of these samples has decreased. However, their large hysteresis loop appears at a relative pressure P/P_0 of 0.80–0.90 in the isotherms, which reveal uniform mesopores with a narrow pore size.

The insert of Fig. 4 shows that the similar the small mesopore with mean pore size of around 2.9 nm for all samples a, b and c, the large pore size decreases from 20 nm for BMMs, to 17.8 nm for APTES-BMMs, and to 16.6 nm for LHBMS-10, indicating the presence of a bimodal mesopores after post-treatment, and then grafting of the surface with the functional groups. From the results discussed with the evidence of above TEM images, we can conclude that these hybrid materials contain a bimodal mesopore system, and the large mesopores may be contributed by the intra-particle spaces, and the particle size being quite uniform.

With the incorporation of the APTES into BMMs surface, the pore volume of sample b (APTES-BMMs), decreases dramatically from 1.29 to 0.83 cm^3/g, and its BET surface area decreases from 918 to 579 m^2/g as well in Fig. 4 (insert), which implies that the amine groups have been indeed inserted into the mesopore channels of the BMMs [10,11]. Along with the grafting of the 1,8-naphthalic anhydride, the pore volume and the BET surface area of sample c (LHBMS-10) in Fig. 4 (insert) further decrease to 0.73 and 521 m^2/g.

3.4. FT-IR analysis

Fig. 5 shows the FT-IR spectra (4000–400 cm^{-1}) of BMMs (a), APTES-BMMs (b), and LHBMS-10 (c). As can be seen, all samples exhibit strong bands in the 1000–1250 cm^{-1} range, corresponding to the asymmetric Si–O stretching vibration [10]. The peak at 802 cm^{-1} arises from the symmetric Si–O stretching vibration, whereas the peak at 460 cm^{-1} can be assigned to the Si–O–Si bending vibration. The peak at 960 cm^{-1} in Fig. 5a

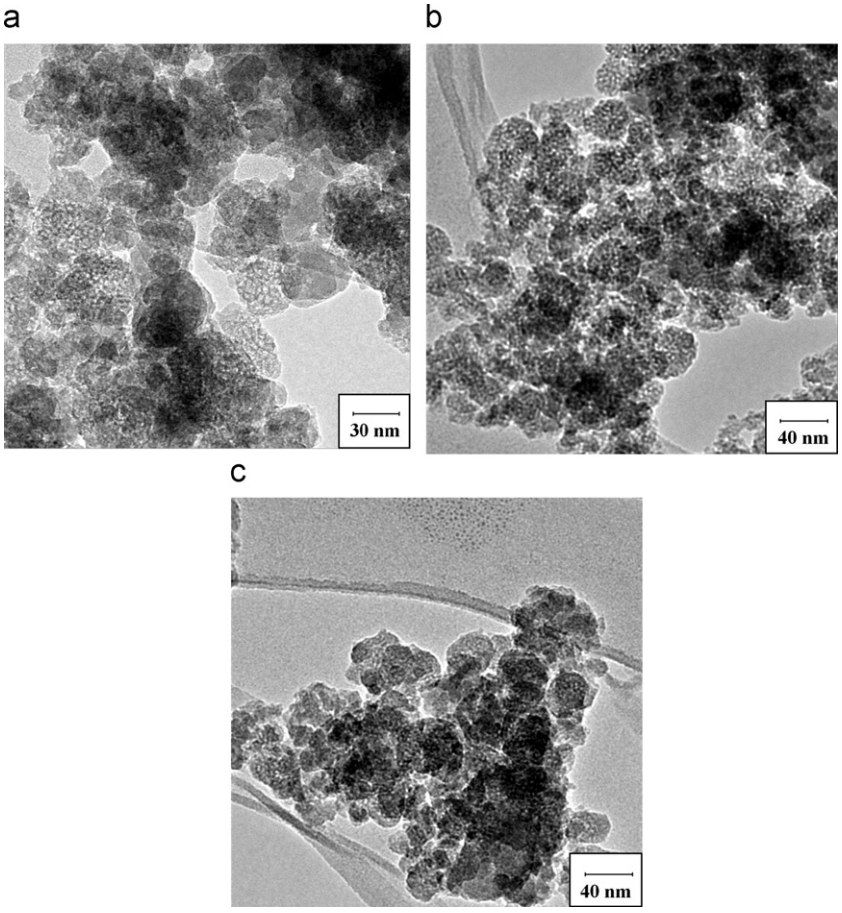

Fig. 3. TEM images of samples, (a) BMMs, (b) APTES-BMMs, and (c) LHBMS-10.

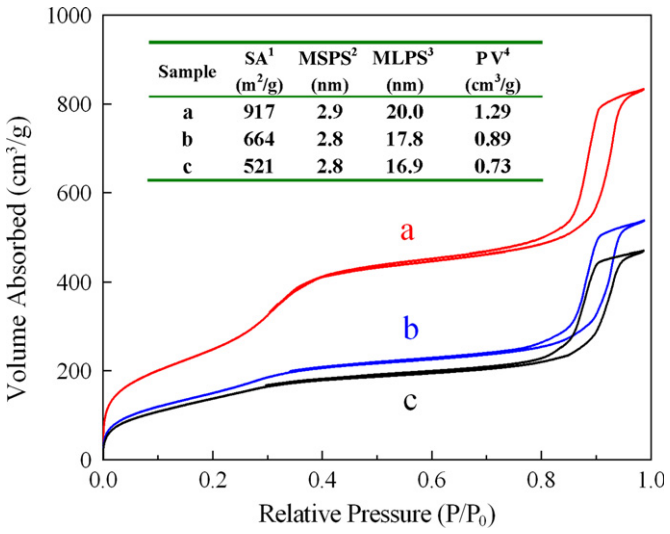

Fig. 4. N_2 adsorption/desorption isotherms of samples, (a) BMMs, (b) APTES-BMMs, (c) LHBMS-10, and texture parameters of samples (insert). *Notes*: SA[1] is the surface area, MSPS[2] the mean small pore size, MLPS[3] the mean large pore size, and PV[4] the pore volume.

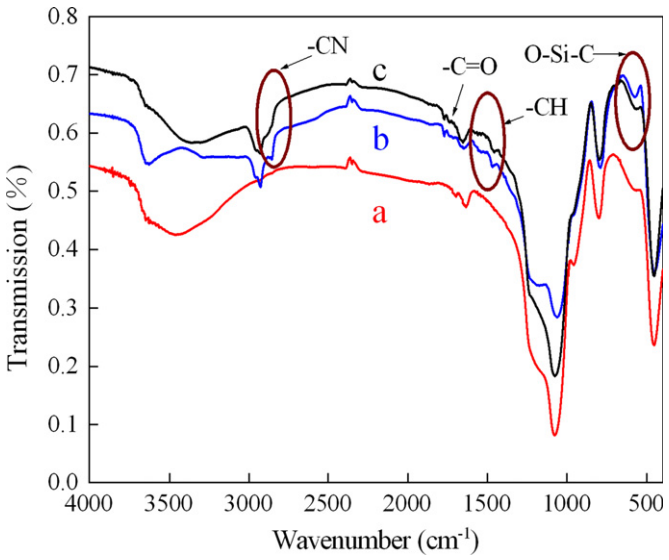

Fig. 5. FT-IR spectra of samples, (a) BMMs, (b) APTES-BMMs, and (c) LHBMS-10.

originates from the stretching vibrations of Si–OH, comparatively, small shift peak at 960 cm^{-1} is observed in Fig. 5b and c, denoting the lack of Si–OH group in samples b and c. In addition, the peaks at 3200, 1417, and 2930 cm^{-1} for samples b and c, indicate the N–H bending, the C–H stretching vibration, and the C–N stretching, respectively, which further confirm the presence of $-CH_2NH_2$ functional group [23,25]. Moreover, the absorption band appearing around 699 cm^{-1} in Fig. 5b belongs to O–Si–C, indicating that the pore surface of BMMs has been successfully modified with the $-Si(CH_2)_3NH_2$ group. Especially, in Fig. 5c, The extra peaks at 1705, 1657, and 1379 cm^{-1}, corresponding to the characteristic absorption band of 1,8-Naphthalic anhydride, imply

that the luminescent groups have been grafted into pore channel of hybrid materials in sample c [25,26].

From these observations, it is shown that the functional groups and luminescent molecules can be successfully incorporated into the mesoporous channel of BMMs via post-treatment and grafting method.

3.5. UV–vis analysis

Fig. 6 displays the UV–vis absorption spectra of samples including a: BMMs, b: APTES-BMMs, c: 2-[3-(triethoxysilyl) propyl-1 H-Benz [de]isoquinoline-1, 3(2 H)-dione, and d: LHBMS-10. As shown in Fig. 6c, the fluorescent molecule shows a narrow adsorption at 240 nm and a broad adsorption band centered at 335 nm. After being introduced into the APTES-BMMs with functional group (sample d), there is no obvious change of the characteristic peak (in Fig. 6d), Meantime, it is worth noticing that there is no adsorption peak in the range of 200–800 nm for samples a and b (seen in Fig. 6a and b). Therefore, it can be easily concluded that the adsorption peaks of LHBMS-10 in Fig. 6c result from the incorporation of luminescent molecule [26].

3.6. Photoluminescence analysis

The emission properties of samples (a 2-[3-(triethoxysilyl) propyl-1 H-Benz [de]isoquinoline-1, 3(2 H)-dione, b LHBMS-10) are investigated in the solid state at room temperature. Both the samples show a strong emission band between 400 and 500 nm upon excitation at 300 nm in Fig. 7, suggesting that these emission lines are due to the primary transition present in the functional groups of the fluorescent materials. In Fig. 7a, one well-resolved emission band can be easily observed with a maxima at about 464 nm [26], which is attributed to π–π^* character of the S_0–S_1 transition. After loading on APTES-BMMs, the emission spectra of sample b (in Fig. 7b) were distinctly blue-shifted to lower wavelength with a maxima at 444 nm, which is more symmetric than that of 2-[3-(triethoxysilyl) propyl-1 H-Benz [de]isoquinoline-1, 3(2 H)-dione, meaning the existence of quantum confinement effectiveness, and the possible interactions between the fluorescent molecule and the surface of the mesopore. These results are consistent with other luminescent dye dispersed in the mesopore reported previously

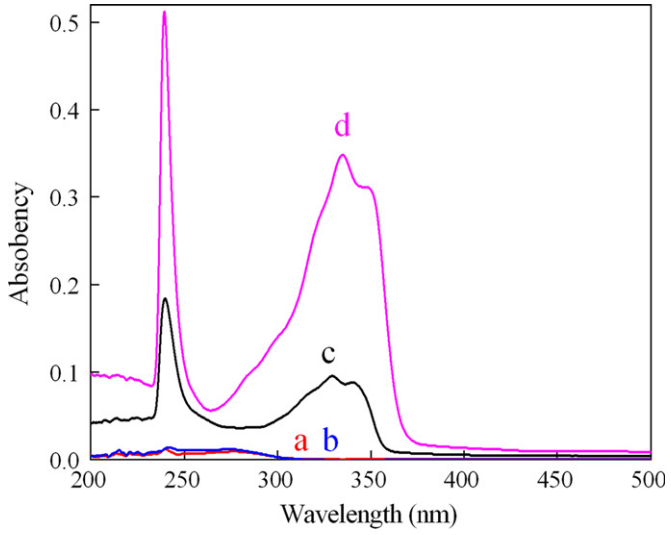

Fig. 6. UV–vis absorption spectra of samples, (a) BMMs, (b) APTES-BMMs, (c) 2-[3-(triethoxysilyl) propyl-1H-Benz [de]isoquinoline-1, 3(2H)-dione, and (d) LHBMS-10.

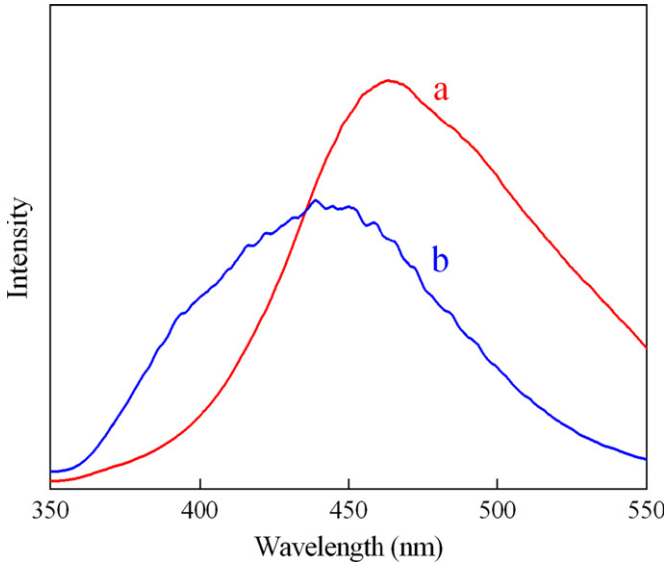

Fig. 7. Emission spectra of (a) 2-[3-(triethoxysilyl) propyl-1H-Benz [de]isoquinoline-1, 3(2H)-dione and (b) LHBMS-10.

[27,28]. When the organic molecules were introduced into the mesopores channel, they were very difficult to aggregate in the mesoporous channels of BMMs, and therefore fluorescent molecules should be highly dispersed as similar to monomers, which is beneficial to increase the fluorescent molecule energy between the ground state and the excited state [29].

4. Conclusions

In summary, we have successfully synthesized novel luminescent hybrid mesoporous silicas by the incorporation of 1,8-Naphthalic anhydride into the mesoporous channels of BMMs. The XRD patterns and TEM images reveal that the organic groups have been successfully introduced into the mesopores of the BMMs without disrupting the mesostructure after the incorporation of the functional groups. The N_2 sorption data indicate that the pore size, surface area, and the pore volume of LHBMS decrease in comparison to BMMs. FT-IR and UV–vis spectra identify the structural coordination of the organic complex and the mesoporous silica matrix. The PL spectra, which are used to characterize the optical behavior of samples, show that the characteristic wavelength of LHBMS has a blue shift as compared with that of 2-[3-(triethoxysilyl)propyl-1 H-Benz[de]isoquinoline-1,3(2 H)-dione, suggesting the existence of the quantum confinement effectiveness.

Acknowledgments

This work was supported by the National Natural Science Foundation of China (20851002) and the State Basic Research Project (973 Program 2009CB930200).

References

[1] M. Gonzalez, A. Galano, J. Rieumont, T. Lopez, D. Dupeyron, L. Albaran, J. Phys. Chem. C 112 (2008) 20222–20226.
[2] K. Pirjo, A. Manja, K. Minna, K. Ilkka, Y Antti, K. Juha, Int. J. Pharm. 200 (2000) 223–229.
[3] C.W. Lam, J.T. James, R. McCluskey, R.L. Hnter, Toxicol. Sci. 77 (2004) 126–134.

[4] A.P. Pietropaoli, M.W. Frampton, R.W. Hyde, P.E. Morrow, G. Oberdörster, C. Cox, D.M. Speers, L.M. Frasier, D.C. Chalupa, L.S. Huang, M.J. Utell, Inhal. Toxicol. 16 (2004) 59–72.
[5] C.T. Kresge, M.E Leonowicz, W.J. Roth, J.C. Vartuli, J.S. Beck, Nature 359 (1992) 710–712.
[6] B.L. Newallkar, N.V. Choudary, P. Kumar, S. Komarneni, T.S.G. Bhat, Chem. Mater. 14 (2002) 304–309.
[7] S.E. Park, R. Ryoo, W.S. Ahn, C.W. Lee, R. Chang (Eds.), Nanotechnology in Mesostructured Materials, 146, Elsevier, Amsterdam, 2003, pp. 1–815.
[8] C. Nozaki, C.G. Lugmair, A.T. Bell, T.D. Tilley, J. Am. Chem. Soc. 124 (2002) 13194–13203.
[9] X. Chen, A.L Rogach, D.V. Talapin, H. Fuchs, L. Chi, J. Am. Chem. Soc. 128 (2006) 9592–9593.
[10] A.S. Maria Chong, X.S. Zhao, J. Phys. Chem. B 107 (2003) 12650–12657.
[11] L. Gao, J.H. Sun, Acta Petrolei Sin. (Pet. Process. Sect.) 22 (2006) 265–268.
[12] W. Wang, D.L. Shi, Appl. Phys. Lett. 89 (2006) 183106–183108.
[13] A. Wada, S. Tamaru, M. Ikeda, I. Hamachi, J. Am. Chem. Soc. 131 (2009) 5321–5330.
[14] S. Park, T.A. Taton, C.A. Mirkin, Science 295 (2002) 1503–1506.
[15] B. Dubertret, P. Skourides, D.J. Norris, V. Noireaux, A.H. Brivanlou, A. Libchaber, Science 298 (2002) 1759–1762.
[16] X. Wu, H. Liu, J. Liu, K.N. Haley, J.A. Treadway, J.P. Larson, N. Ge, F. Peale, M.P. Bruchez, Nat. Biotechnol. 21 (2003) 41–46.
[17] J.K. Jaiswal, H. Mattoussi, J.M. Mauro, S.M. Simon, Nat. Biotechnol. 21 (2003) 47–51.
[18] D.R. Larson, W.R. Zipfel, R.M. Williams, S.W. Clark, M.P. Bruchez, F.W. Wise, W.W. Web, Science 300 (2003) 1434–1436.
[19] E.B. Voura, J.K. Jaiswal, H. Mattoussi, S.M. Simon, Nat. Med. 10 (2004) 993–998.
[20] H. Cao, V. Chang, R. Hernandez, M.D. Heagy, J. Org. Chem. 70 (2005) 4929–4934.
[21] W.H. Zhang, X.B. Lu, J.H. Xiu, Z.L. Hua, L.X. Zhang, M. Robertson, J.L. Shi, D.S. Yan, J.D. Holmes, Adv. Funct. Mater. 14 (2004) 544–551.
[22] C. Debraj, Y. Toshiyuki, T. Takashi, B. Asim, Chem. Mater. 19 (2007) 5347–5354.
[23] Q.G. Meng, P. Boutinaud, A.C. Franville, H.J. Zhang, R. Mahiou, Microporous Mesoporous Mater. 65 (2003) 127–136.
[24] P.I. Ravikovitch, Alexander V. Neimark, Colloids Surf. A 187–188 (2001) 11–21.
[25] C.Y. Peng, H.J. Zhang, J.B. Yu, Q.G. Meng, L.S. Fu, H.R. Li, L.N. Sun, X.M. Guo, J. Phys. Chem. B 109 (2005) 15278–15287.
[26] R. Enriro, B. Elena, M. Silvia, M. Fabrizio, T. Paolo, T. Umberto, J. Mater. Chem. 15 (2005) 2687–2696.
[27] N. Li, X.T. Li, W. Wang, W.C. Geng, S.L. Qiu, Mater. Chem. Phys. 100 (2006) 128–131.
[28] O. Makoto, N. Tomoyuki, M. Jun-ichi, K. Kazuyuki, J. Phys. Chem. B 104 (2000) 8554–8556.
[29] G.D. Chen, L.Z. Wang, J.L. Zhang, F. Chen, M. Anpo, Dyes Pigm. 81 (2009) 119–123.